Steel and Composite Structures, *Vol. 31, No. 1 (2019) 1-12*
DOI: https://doi.org/10.12989/scs.2019.31.1.001

Structural behavior of the stiffened double-skin profiled composite walls under compression

Ying Qin*, Yong-Wei Li, Xu-Zhao Lan, Yu-Sen Su, Xiang-Yu Wang and Yuan-De Wu

Key Laboratory of Concrete and Prestressed Concrete Structures of Ministry of Education, and National Prestress Engineering Research Center, School of Civil Engineering, Southeast University, Nanjing, China

(*Received June 25, 2018, Revised February 1, 2019, Accepted March 16, 2019*)

Abstract. Steel-concrete composite walls have been proposed and developed for applications in various types of structures. The double-skin profiled composite walls, as a natural development of composite flooring, provide structural and architectural merits. However, adequate intermediate fasteners between profiled steel plates and concrete core are required to fully mobilize the composite action and to improve the structural behavior of the wall. In this research, two new types of fasteners (i.e., threaded rods and vertical plates) were proposed and three specimens with different fastener types or fastener arrangements were tested under axial compression. The experimental results were evaluated in terms of failure modes, axial load versus axial displacement response, strength index, ductility index, and load-strain relationship. It was found that specimen with symmetrically arranged thread rods sustained more stable axial strain than that with staggered arranged threaded rods. Meanwhile, vertical plates are more suitable for practical use since they provide stronger confinement to profiled steel plate and effectively prevent the steel plate from early local buckling, which eventually enhance the composite action and increase the axial compressive capacity of the wall. The calculation methods were then proposed and good agreement was observed between the test results and the predicted results.

Keywords: profiled composite wall; compressive loading; structural performance; strength; strain analysis

1. Introduction

Normally, brick walls or reinforced concrete walls serve to carry gravity load in many structures. However, extensive studies show that these walls exhibit poor ductility and are vulnerable to crashing (Sakr *et al*. 2017). Meanwhile, cold-formed rectangular hollow section has been increasingly applied due to the reasonable section shape, good mechanical properties, and high steel utilization (Qin and Chen 2016, Qin *et al*. 2018a, Liu *et al*. 2018). The behavior under air-blast loading (Ritchie *et al*. 2018), local buckling (Garifullin *et al*. 2018), imperfection sensitivity (Shen and Wadee 2018), temperature distribution (Bqczkiewicz *et al*. 2018), and the design method (Choi and Kwon 2018) have been investigated by several researchers. However, hollow sections are vulnerable to local buckling (Qin *et al*. 2018b, c). The combination with infill concrete to construct concrete-filled section thus is good choice to significantly enhance the performance (Qin *et al*. 2015a, b, 2016). Recently, double-skin steel-concrete composite wall, which consists of two skins of steel plate and an infill of concrete, has increasingly attracted attention.

This type of wall owns advantages over traditional reinforced concrete walls to resist axial loading. In the construction stage, the external steel plates act as the permanent formwork for infill concrete and can also serve as the bracing system to the building frame against lateral loads such as wind. In the service stage, the steel plates are considered also as reinforcement and as well offer lateral restraint to concrete infill, which put the concrete in a tri-axially compressive state and largely increases the bearing capacity. Meanwhile, the concrete core provides strong confinement to profiled steel plate and prevent the plate from buckling inwards, and the internal fasteners prevent the plate from buckling outwards. In this way, the profiled steel plate and the concrete infill can work together to comprise a composite wall to resist axial loading.

On the other hand, profiled composite walls possess greater compressive buckling strength as well as higher load-bearing capacity when compared with flat double skin composite walls, due to the profiled configuration.

Therefore, this wall has the potential to act as bearing walls to resist compressive loading in modern, sustainable, and lightweight building structures. It possesses significant composite action between profiled steel plate and concrete core and can be applied to safety facilities such as nuclear power plants due to its unique materials.

Many researchers focus on the double-skin flat steel plate composite walls. Liang *et al*. (2004) used finite element method to obtain the local and postlocal buckling strength of steel plates in composite walls under biaxial compression and in-plane shear. Aykac *et al*. (2014) studied the effect of external steel plate on the loading capacity, ductility, and rigidity of hollow brick infill walls under monotonic diagonal compressive loading. Zhang *et al*. (2014) investigated the influence of shear connector on the

*Corresponding author, Ph.D., Associate Professor, E-mail: qinying@seu.edu.cn

http://www.techno-press.org/?journal=scs&subpage=6
ISSN: 1229-9367 (Print), 1598-6233 (Online)

level of composite action and development length of steel plate in composite walls. Choi *et al*. (2014) described the compressive performance and determined the squash load of composite walls using ordinary and eco-oriented cement concrete. Epackachi *et al*. (2015) proposed an analytical model to analyze the structural behavior of composite walls. The monotonic load-displacement response of the walls can be accurately predicted by this method. Huang and Liew (2016) studied the steel-concrete-steel composite wall with J-hook connector. The research indicated that the J-hook connector played an important role in providing composite action between the steel plate and the concrete, and delaying or preventing local buckling of the external steel plate. Qin *et al*. (2017a) proposed calculation method for the compressive strength of double skin composite walls. Recently, Qin *et al*. (2019a, b) experimentally investigated the axial behavior of full-scaled double skin composite walls with different height-thickness ratios and plate thicknesses.

The concept of double-skin profiled steel plate composite walls comes from the widely-used composite floor system using profiled steel deck and concrete. This new type of walls offers substantial merits when used in conjunction with composite flooring, which includes increased strength, stiffness, and ductility for both compressive and flexural modes of failure. In addition, the use of profiled composite walls reduces wall thickness and lead to increased floor areas in buildings (Qin *et al*. 2019c).

This type of composite wall can be used as structural load-bearing walls in low-rise residential building when using lightweight foamed concrete (Mydin and Wang 2011, Prabha *et al*. 2013) and in mid-rise and tall building when using ordinary concrete, self-consolidating concrete and highly ductile engineered cementitious composite (Hossain *et al*. 2016).

It is of importance to investigate the compressive behavior of this type of wall. On the one hand, this wall may be applied to projects (such as non-load-bearing walls, load-bearing walls in low-rise buildings, and gravity seawalls) where only compressive loading is applied or compressive loading is the dominant force. On the other hand, the high bearing capacity of this wall requires the cooperative performance between the steel plate and concrete. However, the local buckling of steel plate may lead to poor composite action, which has significant influence on the axial compressive performance of composite walls. Due to the small thickness of profiled steel plates, the weakening effect on compressive strength caused by local buckling may be significant.

The axial load capacity of the profiled composite wall was found to be dependent upon the capacity of the concrete and steel and the transfer of load between the two (Wright 1998). The lack of effective connection between the steel plate and concrete led to a poor composite behavior and a reduced axial compressive capacity of the composite wall. The recent studies by Hilo *et al*. (2016) and Yousefi and Ghalehnovi (2018) also indicated that the axial load resisting capacity of the wall is significantly influenced by the early local buckling of the profiled steel plate, followed by the concrete crash. The imperfect steel-concrete interface bonding is an essential deficiency of the composite systems that resulted in separation between steel and concrete surfaces under compressive and lateral loads (Shekastehband *et al*. 2018). In order to increase the load resistance, the local buckling of the profiled steel plates should be prevented. Adequate intermediate fasteners such as J-hook connectors (Wright 1998, Rafiei *et al*. 2013), binding bars (Prabha *et al*. 2013, Hossain *et al*. 2016), embedded cold-formed steel tubes (Hilo *et al*. 2016), headed studs (Uy *et al*. 2001, Yan *et al*. 2018) should be used along the height and width of the composite wall to enhance the composite action between the profiled steel plates and concrete.

Previous studies demonstrated that in order to fully mobilize the composite action and the improve the structural behavior of the wall, appropriate load transfer devices in terms of embossments or other mechanical connections between profiled steel plates and concrete are required. In most studies reported in literature, the profiled steel plates and concrete were connected only at the boundary surface, which led to premature local buckling of steel plates. In addition, no variability in the arrangements and types of fasteners was evaluated.

In this paper, two new forms of fasteners are proposed to connect the profiled steel plates and concrete core to improve the composite action. The present research aims to investigate the fundamental performance and load bearing capacity of these new profiled composite walls subjected to axial compressive loading with different arrangements of interconnection devices.

2. Experimental program

2.1 Test specimen

Three profiled composite wall specimens were tested under compressive loading. The configurations of profiled steel plate and the wall dimensions are shown in Figs. 1 and 2, respectively. The dimensions of the profiled steel plate and the wall are the same for all specimens. The type of profiled steel plate is YX35-125-750 with the thickness of 1.2 mm. The wall dimensions are 800 mm high, 520 mm wide, and 180 mm thick, which results in the slenderness ratio of 4.44 for all specimens. Consequently, the tested specimens are classified into short wall category and the failure mode of the specimens is expected to be controlled by the cross-sectional capacity.

While keeping the parameters above constant, the patterns of intermediate fasteners are varied in the three composite wall specimens. The general arrangements of specimens are illustrated in Fig. 3. Out of three specimens, the first two specimens (Specimens DKCW-1 and DKCW-2) use threaded rod to act as the steel plate-concrete interface connection. The threaded rods, with a diameter of 10 mm and a length of 80 mm, are arranged at a distance of 125 mm along both the height and width of the composite wall on each side. The threaded rods in Specimen DKCW-1 are arranged at the same locations on two opposite steel plates, while those in Specimen DKCW-2 are staggered

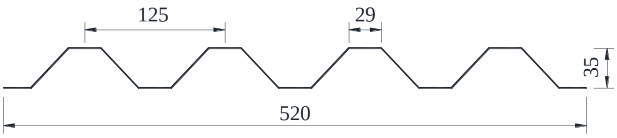

Fig. 1 Configuration of profiled steel plate

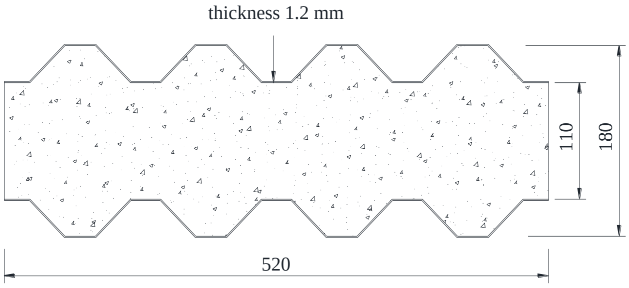

Fig. 2 Dimension of the profiled composite wall

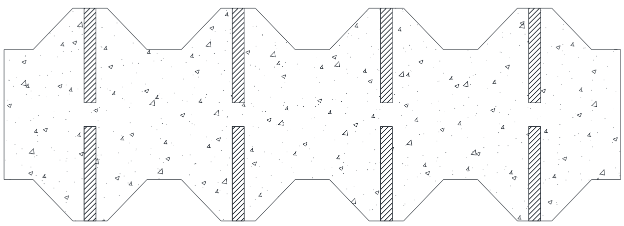

(a) Specimen DKCW-1

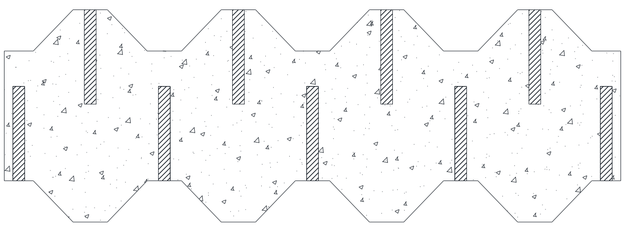

(b) Specimen DKCW-2

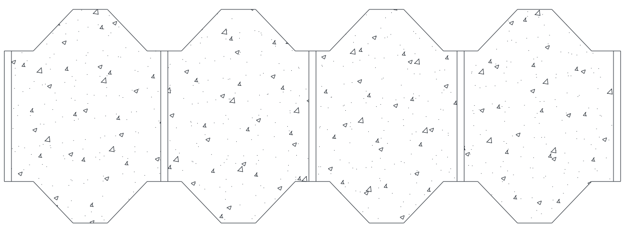

(c) Specimen DKCW-3

Fig. 3 General arrangements of specimens

arranged. Specimen DKCW-3 uses vertical plates to connect the two profiled steel plates. The thickness of the vertical plates is 6 mm, and the spacing between the vertical plates is 125 mm along the width of the wall.

2.2 Material properties

In order to obtain the material properties of cold-formed profiled steel plate, three tension coupon specimens are

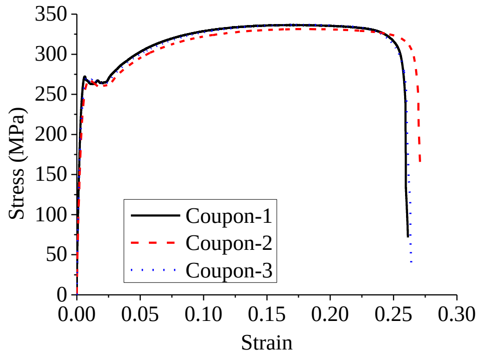

Fig. 4 Stress-strain response of profiled steel plate

Table 1 Material properties of profiled steel plate

Specimen No.	Thickness	Young's modulus	Yield strength	Ultimate strength	Elongation
	mm	GPa	MPa	MPa	%
Coupon-1	1.2	2.06×10^2	264.5	336.5	26.1
Coupon-2	1.2	1.92×10^2	260.9	331.5	27.1
Coupon-3	1.2	2.00×10^2	264.7	336.8	26.4

made from the same batch of profiled steel plates used for the test specimens. The stress-strain response of the steel is shown in Fig. 4. The material properties of steel determined from coupon test are given in Table 1. The averaged yield and ultimate stress of steel is 263.4 MPa and 334.9 MPa, respectively and the Young's modulus is 1.99×10^2 GPa. Three cubes with the dimension of 150×150×150 mm are cast for concrete and tested on the day of testing the wall specimens. The averaged cubic strength of cubes is 24.0 MPa. According to Code for design of concrete structures (GB50010-2010, 2015), the corresponding cylinder strength is 18.24 MPa.

2.3 Test setup and instrumentation

The profiled composite walls were tested under axial compressive loading with the 2000 kN testing machine at Southeast University, as shown in Fig. 5. Three linear varying displacement transducers were placed at the bottom of the wall to record the axial deformation under compression. Forty strain gauges were arranged to monitor the strain development during the test, as shown in Fig. 6. Three rows of strain gauges on each side (Side A and Side B) were mounted at a distance of 100 mm, 400 mm, 700 mm from the bottom of the wall, respectively, to measure the strains along the height. One another row of strain gauges was arranged 250 mm from the bottom on both sides to measure the lateral strains due to the Poisson effect. All strain gauges were numbered with two numbers. For the strain gauges to record the axial strain, the first number denotes the row number, while the second represents the column number. The strain gauge A-22 means the axial strain gauge is in row two column two on Side A. For the strain gauges to record the lateral strain, the first number is set to zero to distinguish from the axial strain gauges, while the second number also stands for the column number. Fine

Fig. 5 Test setup

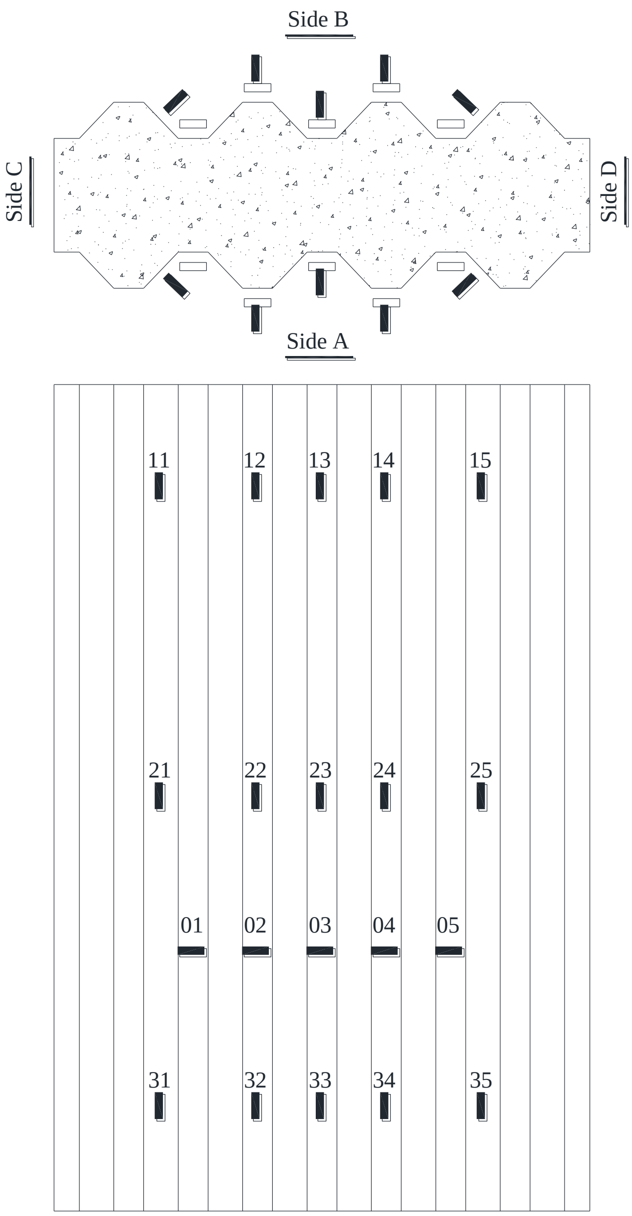

Fig. 6 Arrangement of strain gauges

sand was paved at the top of the specimens to ensure the compressive loading was uniformly transferred to the whole cross section. The load was applied at intervals of 50 kN in order to record the data and observe the deformation. The vertical displacement of the walls and the local buckling of profiled steel plates were properly recorded during the tests.

3. Experimental investigations

3.1 Failure of test specimens

Specimen DKCW-1 behaved in a smooth manner during the loading process. The compressive loading gradually increased with no apparent physical phenomenon observed. When the load reached 450 kN, small but continuous sound was emitted from the specimen. The profiled steel plate, which is on the exposed side B without confine edge, slightly buckled outward 150 mm down from the top. This caused obvious vertical separation of outer steel plate from the concrete. As the load progressed to 650 kN, the separation between steel and concrete became more severe, and small cracks were observed in the concrete on both exposed sides. At the loading level of 1000 kN, obvious buckling waves can be found between the welding spot on the profiled steel plates on both sides, as shown in Fig. 7(a). As the load arrived at 1260 kN, the crack on side B of concrete grew rapidly and the profiled steel plates buckled severely. The specimen reached its ultimate compressive capacity as the load reached 1330 kN and the corresponding axial displacement was 0.72 mm. As the test progressed, the load started to decrease gradually, while the axial deformation continued to grow. When the load dropped to 750 kN, the concrete on both unconfined sides began to peel off, and the buckling waves between the threaded rods were becoming more severe. The failure photograph of Specimen DKCW-1 is given in Fig. 7(b).

Specimen DKCW-2 exhibited similar behaviour to Specimen DKCW-1 at the beginning of the test. The axial displacement steadily increased as the load went on. When the load arrived at 550 kN, non-stop small sound was emitted from the specimen. Simultaneously, the profiled steel plate on side B started to bulge outward at the middle height of the wall and slightly separate from the concrete at the same location. As the load continued growing to 750 kN, big sound was emitted from the specimen. The profiled steel plate on side A began to buckle when the load reached 800 kN. Greater sound was emitted at the load level of 900 kN, and transverse crack developed quickly on the exposed side C of the concrete. As the load grew up to 1100 kN, obvious local crippling can be observed on the profiled steel plate. The concrete at both exposed unconfined sides experienced noticeable damage and large amount of vertical cracks occurred. The damage to concrete caused the load transferred to the steel, which induced significant buckling of steel plate. The specimen reached its ultimate compressive loading capacity as the load arrived at 1260 kN. The corresponding axial displacement was 0.64 mm. The load then began to drop as the axial displacement continued to increase. The concrete at both exposed sides peeled off severely as shown in Figs. 7(c) and (d). The

(a) Buckling wave

(b) Specimen failure

(c) Cracks at Side D

(d) Cracks at Side C

(e) Failure of specimen

(f) Slight buckling

Fig. 7 Failure of test specimens

failure photograph of the specimen is given in Fig. 7(e).

During the test of Specimen DKCW-3, no apparent physical damage was observed. Only slight sound was heard and slight local buckling of profiled steel plate was observed, as given in Fig. 7(f). The ultimate loading capacity of the specimen was 1480 kN and the corresponding displacement was 0.6 mm.

As can be seen from the description above, there are two types of failure modes observed from the test. The first type of failure mode is crack occurring in concrete, followed by the local buckling of profiled steel plates. Subsequently, the profiled steel plates are noticeably separated from the concrete in the vertical direction on both exposed sides of specimens without confined edges. This type of failure initiated combined cracks and vertical separation on the sides of the composite wall. The transferring of compressive load from the crushed concrete to the profiled steel plates induced local buckling of steel plate at the level of crack and local crippling of steel plate perpendicular to the crack while along the width of the wall. Both Specimens DKCW-1 and DKCW-2 with unconfined edges fail in this type of mode. The second type of failure is cross-sectional capacity failure. This type of failure is observed in Specimen DKCW-3. Due to the good confinement that the vertical plates provide, no separation between the profiled steel plates and the concrete is found in this specimen. The concrete is completely cracked and the profiled steel plates are completely yielded. Both materials reached their bearing capacities.

3.2 Load-displacement response

The responses of axial compressive load versus overall axial displacement of the profiled composite walls are shown in Fig. 8. All three specimens exhibited similar load-displacement behavior. The curves go up almost linearly

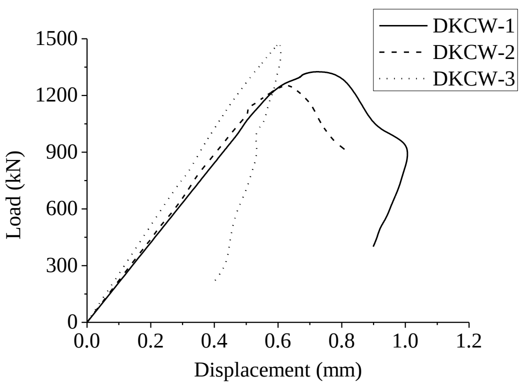

Fig. 8 Load-displacement curve

at the first stage of loading, which indicates that the specimen is in the elastic range. Subsequently, the slopes of the curves gradually decrease, which means the plastic deformation is developing in the specimen. It is evident from the plot that the specimen with vertical plates as the fasteners to connect the steel plate and concrete (i.e., Specimen DKCW-3) enables to sustain higher load bearing capacity. Further-more, comparing with Specimen DKCW-1, Specimen DKCW-2 with staggered threaded rod showed poorer deformation ability. This may due to the fact that severe damage to concrete was observed in the test of Specimen DKCW-2.

In order to quantify the effects of the variables on the axial stiffness of the test specimen, the initial axial stiffness K_i is calculated. Three types of axial stiffness are calculated and the average value was chosen to eliminate random error. The first one takes the origin point as the starting point and the point corresponding to $0.1F_u$ as the terminal point. The second takes the origin point as the starting point and the point corresponding to $0.2F_u$ as the terminal point. While the third takes the origin point as the starting point and the point corresponding to $0.3F_u$ as the terminal point. The initial axial stiffnesses K_i of the three specimens are 2108.1 kN/mm, 2205.7 kN/mm, and 2558.6 kN/mm, respectively. It can be seen that the influence of different arrangements of threaded rods on the axial stiffness is not significant, while the use of vertical plates can largely increase the loading carrying ability under the same level of axial deformation.

3.3 Strength index (SI)

Strength index (SI) is used to assess the bearing capacity and the composite action between profiled steel plate and concrete while exclude the influence caused by the differences in cross-sectional dimensions and steel ratio among specimens. SI can be defined as given by Eq. (1). It should be noted that the factor of 0.85 has been adopted by AISC 360-16 (2016) and Eurocode 4 (EN 1994-1-1 2005). It has also been employed by several researchers (Huang and Liew 2016, Xiong *et al*. 2017) in calculating SI.

$$SI = \frac{N_{u,test}}{0.85A_c f_c' + A_s f_y} \tag{1}$$

where $N_{u,test}$ = ultimate compressive capacity obtained from tests; A_c, A_s= cross-sectional area of concrete and profiled steel plate, respectively; f_c'= compressive strength of concrete; and f_y= yield strength of steel.

The strength index SI of Specimens DKCW-1, DKCW-2, and DKCW-3 calculated by Eq. (1) are 0.829, 0.785, and 0.953, respectively. This indicates that the cross-sectional capacities of the first two specimens are not fully utilized. On the contrast, specimen DKCW-3 makes good use of its materials and exhibits satisfactory bearing capacity. This is due to the different failure modes observed in the test. In Specimens DKCW-1 and DKCW-2, the profiled steel plate may not reach its yield strength due to the fact that, the shedding of load from the cracked concrete to the profiled steel plate causes early local buckling of plate, which hinders the steel to achieve its yield strength. Meanwhile, the concrete core in these two specimens may also not reach its compressive strength due to: (1) stress concentration at the interface between the fastener and the surrounded concrete induces initial local failure of concrete under compressive loading; (2) the profiled geometry of the section may lead to the reduction in concrete capacity if the bond between the steel and concrete is incomplete and insufficient.

3.4 Ductility index (DI)

Ductility index (DI) is an important parameter to evaluate the ability of the structure to undergo large plastic deformation without significant loss of strength. Several definitions of ductility index (DI) were used by various researchers based on load versus axial displacement curves (Du *et al*. 2016, Zhang *et al*. 2018), or load versus axial strain curves (Tao *et al*. 1998, Han 2002). The ductility index in terms of displacement can be defined as the ratio of axial shortening at 85% peak load during the descending stage $\Delta_{85\%}$ to axial shortening corresponding to ultimate capacity Δ_u, as expressed by Eq. (2).

$$DI = \frac{\Delta_{85\%}}{\Delta_u} \tag{2}$$

Based on Eq. (2), the ductility index for Specimens DKCW-1 and DKCW-2 are 1.199 and 1.148, respectively.

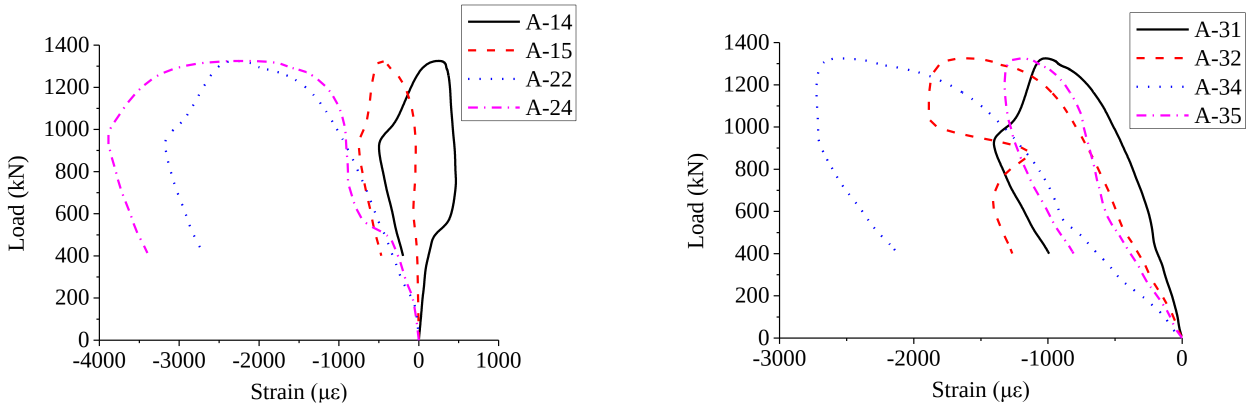

Fig. 9 Load-strain response of Specimen DKCW-1

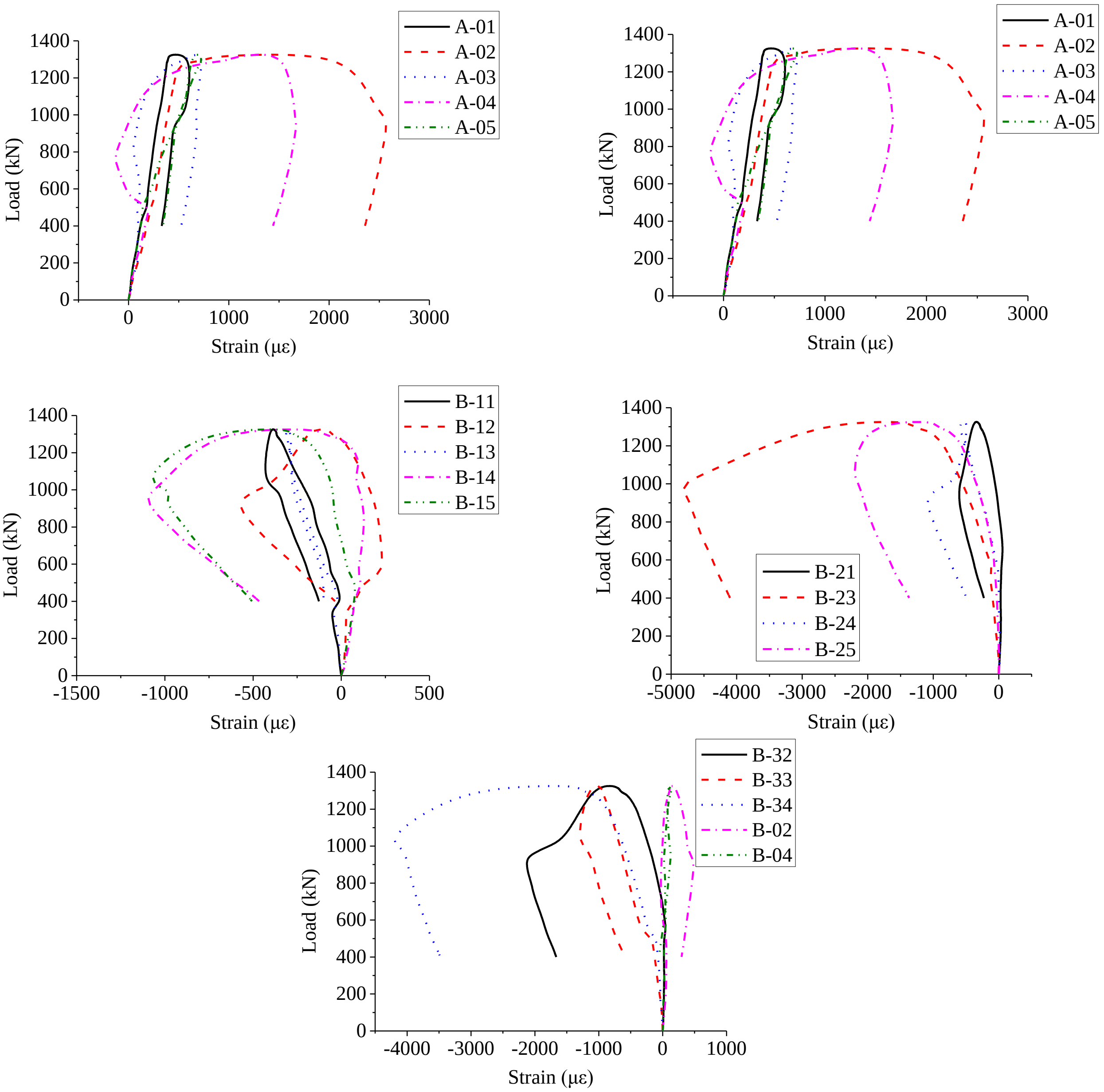

Fig. 9 Continued

The specimen with staggered threaded rod has lower ductility index because the specimen suffers more from the concrete crushing. It should be noted that the ductility index for Specimen DKCW-3 is not available due to the fact that the stiffness of the setup (loading frame) is not enough to sustain the descending stage for this specimen and thus, the loading process is stopped when the peak load is achieved, followed by the unloading process.

3.5 Load-strain response

Figs. 9-11 describe the responses of the axial load versus the profiled steel plate strain for three specimens. The negative value represents the compression, and the positive value denotes the tension.

The strain development in three specimens showed similar trend. The strains increase linearly at the beginning of loading. Most strains do not reach the yield strain even when the specimens reach their peak load, which indicates that the yield strength of the profiled steel plate cannot be used in calculating the compressive capacity of the profiled composite wall. It may be necessary to determine the buckling strength of the steel plate in evaluating the specimen capacity. The descending stage of all the load-strain curves is stable and gradual, which demonstrates the good ductility of the test specimens. During the whole loading process, the increase rate of axial strain is greater than that of the lateral strain before the specimens arrive at their peak load, which demonstrates that the axial shortening is the dominate deformation in this stage. The lateral strains gradually increase after the peak load, chiefly because the profiled steel plates tend to buckle outward rapidly in this stage.

It can be observed that the strains in Specimen DKCW-3

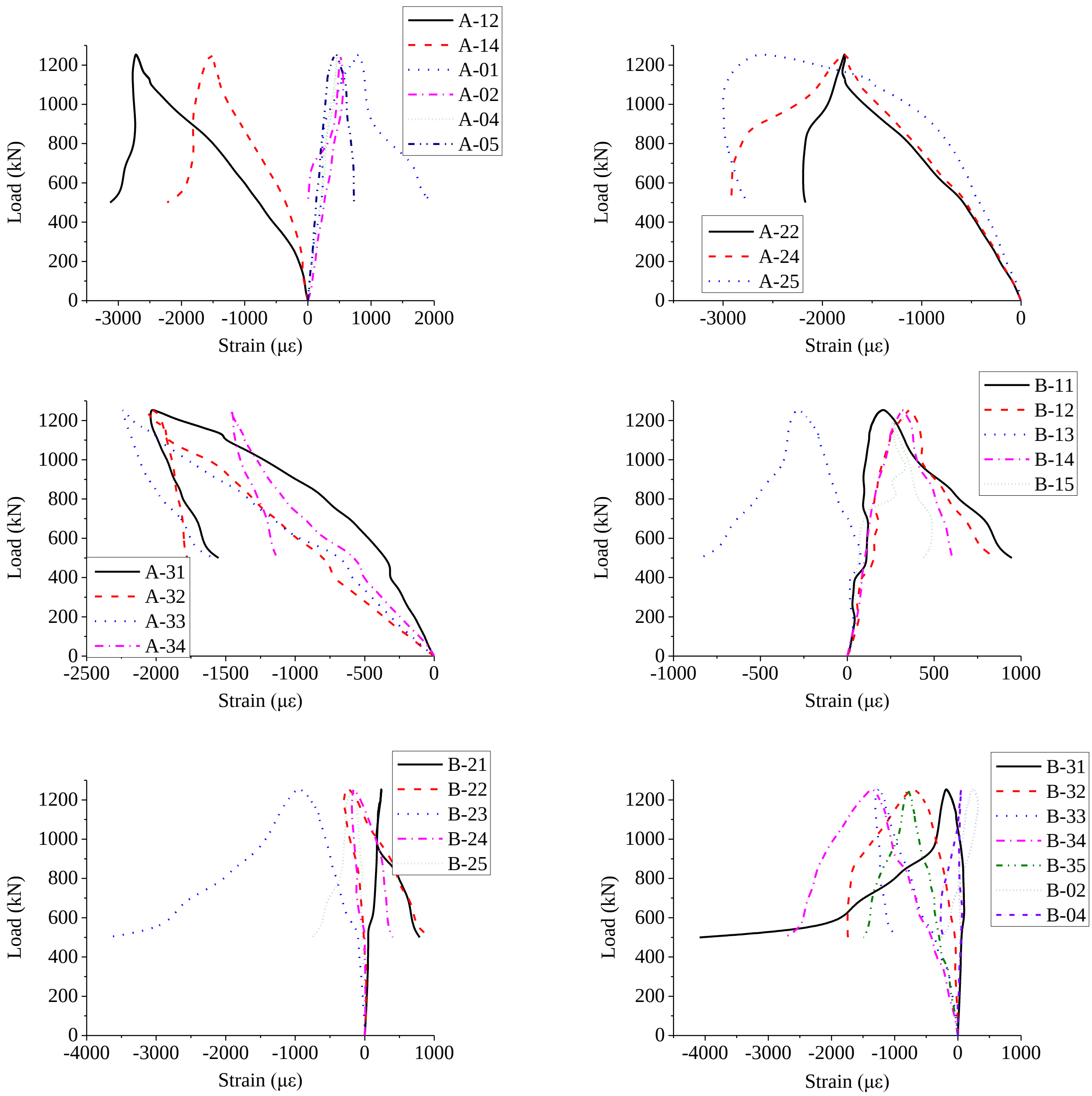

Fig. 10 Load-strain response of Specimen DKCW-2

show almost linear axial strain development up to the peak load point, while the slope of load-strain curves for most strains in the other two specimens gradually decrease with the growth of compressive load. This indicates that the vertical plates in Specimen DKCW-3 provide strong restraint to the profiled steel plates and prevent the steel plates from early buckling, which will delay the local crushing of concrete and thus enhance the composite action between the steel plate and the concrete core. Meanwhile, the threaded rods are able to offer certain bond between steel plate and concrete, but the bond may be not sufficient when the load is significantly high. The comparison of load-strain performance between Specimens DKCW-1 and DKCW-2 shows that, Specimen DKCW-1 exhibits more stable axial deformation than Specimen DKCW-2 does during the descending branch. This means the threaded rod arrangement type in Specimen DKCW-1 is more suitable for practical use as the specimen could undergo greater deformation under compression.

The comparison among three specimens indicates that fewer strains develop in Specimen DKCW-3 than in the other two specimens for strain gauges at the same row under the same loading level. This indicates that due to the better composite action in Specimen DKCW-3, more axial compression is carried by concrete core, which is beneficial as the concrete has high compressive capacity. This can postpone the local buckling of profiled steel plate and thus increase the load-bearing capacity of the wall.

It can also be observed that more strains develop at the edge of the profiled steel plate than in the middle for the strain gauges in the same row. This is attributed to the fact that the concrete offers stronger confinement to the steel

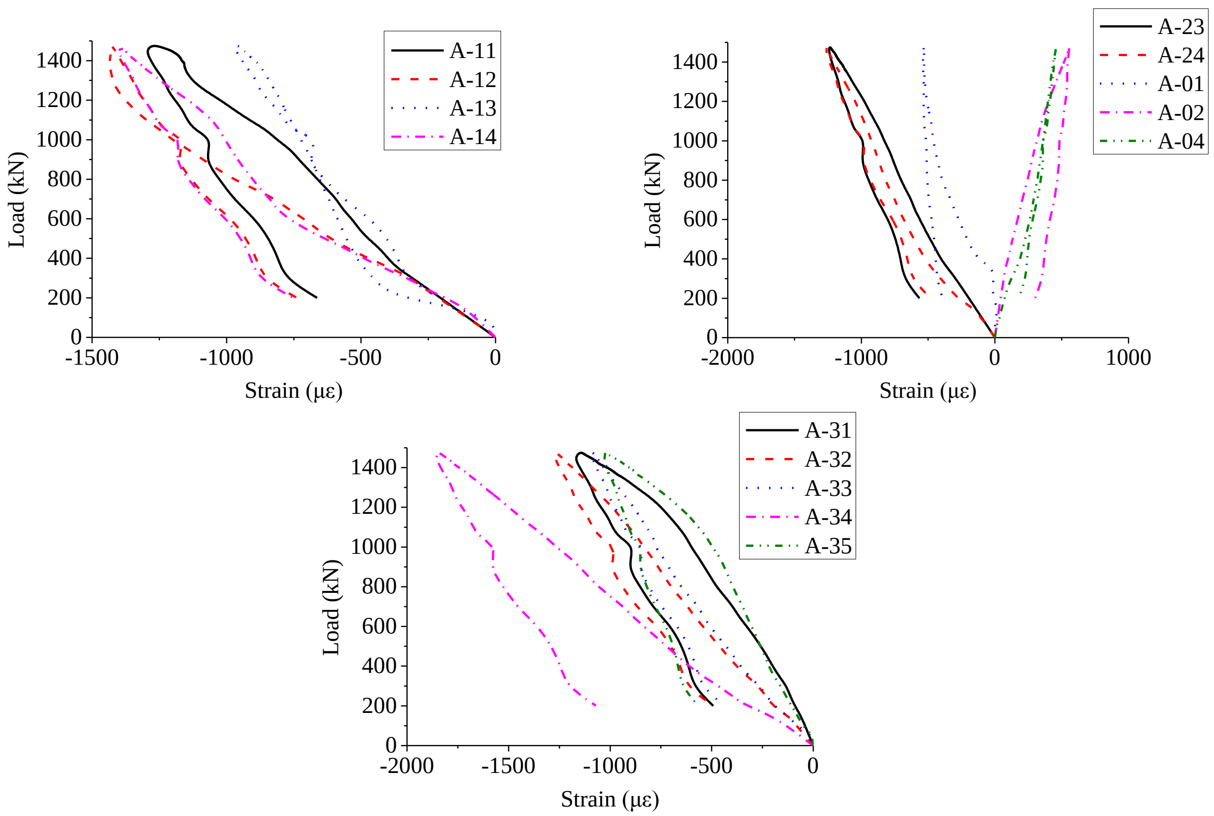

Fig. 11 Load-strain response of Specimen DKCW-3

plate in the middle, while the restraint to the steel plate at the edge is weak, which leads to quickly-developed strains.

Meanwhile, Figs. 9 and 10 show that the strains of Specimens DKCW-1 and DKCW-2 in the same column gradually decrease as the growth in the distance from the loading surface. This demonstrates that the compressive loading applied to steel plate is gradually transferred to the concrete core through fasteners. This may be due to the local buckling of steel plate. The buckled steel plate is not able to sustain the axial compression and forces part of compression is delivered to the concrete. In contrast, Fig. 9 show that the strains in the same column of Specimen DKCW-3 almost uniformly distributed along the height of the walls. This means composite action is better achieved in Specimen DKCW-3.

4. Discussion on calculation methods

4.1 AISC 360-16

Profiled composite walls are classified as slender section in AISC 360-16 (2016). The steel sheet is assumed to reach its buckling strength of f_{cr} rather than its yield strength f_y. Meanwhile, it is considered that the steel cannot provide sufficient confinement to concrete in slender section and thus, the concrete is assumed to only reach the compressive strength of $0.70f_c^{'}$. The expression is shown in Eq. (3).

$$F_{AISC} = f_{cr}A_s + 0.7f_c^{'}A_c \tag{3}$$

where A_c and A_s are the area of concrete infill and steel sheet, respectively. f_{cr} is the critical buckling strength and can be calculated by Eq. (4) for rectangular filled sections.

$$f_{cr} = \frac{9E_s}{(b/t)^2} \tag{4}$$

4.2 EN 1994-1-1

Eurocode 4 (EN 1994-1-1 2004) assumes that the composite wall has sufficient ability to develop yielding of the steel sheet in longitudinal compression, and to offer confinement to the concrete fill to develop its compressive strength of $0.85f_c^{'}$. The calculation expression is given by Eq. (5).

$$F_{Euro} = f_yA_s + 0.85f_c^{'}A_c \tag{5}$$

4.3 CECS 159

CECS 159 (2004) is based on superposition principle. It assumes that the steel sheet could reach its yield strength of f_y while the concrete infill could reach the compressive strength of $f_c^{'}$. The expression is given by Eq. (6).

$$F_{CECS} = f_yA_s + f_c^{'}A_c \tag{6}$$

4.4 Proposed method

As described previously, the test walls can be regarded as short walls since the height to thickness ratios is 4.4.

Experimental investigation also shows that no global instability was found during the test, which means the profiled composite walls failed by cross-sectional capacity. As the profiled steel sheet provides confinement to concrete infill and the concrete prevent the steel sheet from buckling inward, the composite action is achieved and the calculation is based on the traditional composite structural system. Therefore, the ultimate capacity of the profiled composite wall F_{pro} can be given by the superposition of the contribution from steel sheet, concrete infill, and surrounded steel reinforcement.

$$F_{pro} = F_s + F_c + F_{rs} \tag{7}$$

where F_s is the capacity of steel sheet, and F_c is the capacity of concrete infill. F_{rs} is the capacity of surrounded steel reinforcement and can be calculated by multiplying the yield strength by the cross-sectional area. For Specimens DKCW-1 and DKCW-2 with shear studs, F_{rs} is taken as zero.

4.4.1 Steel sheet capacity

Effective width method was used for thin-walled structures to consider the reduced strength due to the local buckling. In this research, the method proposed by Mydin and Wang (2011) was modified to calculate the reduced strength of profiled steel plate. The capacity of steel sheet can then be calculated by

$$F_s = b_{eff}\, t f_y \tag{8}$$

where t is the thickness of steel sheet, and f_y is the yield strength of steel sheet.

Liang and Uy (2000) presented a theoretical study on the post-local buckling performance of steel sheets in concrete-filled thin-walled box columns by performing a material and geometric nonlinear finite element analysis. Two effective width equations were derived based on the results as given by

$$\frac{b_{eff}}{b} = 0.675\left(\frac{\sigma_{cr}}{f_y}\right)^{1/3} \quad \text{for} \quad \sigma_{cr} \le f_y \tag{9}$$

$$\frac{b_{eff}}{b} = 0.915\left(\frac{\sigma_{cr}}{\sigma_{cr} + f_y}\right)^{1/3} \quad \text{for} \quad \sigma_{cr} > f_y \tag{10}$$

where σ_{cr} is the critical local buckling stress and can be expressed by Eq. (11).

$$\sigma_{cr} = \frac{k\pi^2 E_s}{12(1-\upsilon^2)(b/t)^2} \le f_y \tag{11}$$

where υ is the Poison's ratio of steel and can be taken as 0.3, k is the elastic local buckling coefficient which depends on the boundary condition of the steel sheet, and b is the effective width of steel plate.

The values of k for different boundary conditions have been proposed by several researchers. For simply-supported loaded and free unloaded edges (SS), a value of 0.8 was proposed by Uy and Bradford (1996). Meanwhile, Gerard and Becker (1957) proposed a value of 4.0 for simply-supported loaded and unloaded edges. Recently, a value of 5.467 was proposed by Qin *et al*. (2017b) for clamped loaded edges and simply-supported unloaded edges (CS).

4.4.2 Concrete infill capacity

Due to the use of internal fasteners, the composite action between steel sheet and concrete infill can be achieved. Therefore, the concrete infill is considered to develop the compressive strength of $0.85f_c'$. The capacity of concrete fill can be determined by Eq. (12).

$$F_c = 0.85 f_c' A_c \tag{12}$$

4.5 Discussion

The comparison among test results, predictions by modern codes and the proposed method in this paper is shown in Table 2. It can be observed both Eurocode 4 and CECS 159 significantly overestimate the actual capacity of profiled composite walls. The average ratios of the test results to the predictions by these two modern codes are 0.783 and 0.703, respectively. The corresponding standard deviations are 0.018 and 0.016, respectively. The great difference between the test and predicted results is because that the capacity of steel sheet is largely reduced due to the local buckling, which is not considered in both codes. In addition, AISC 360 offers obvious underestimation to the actual capacity, as a result of the lower prediction for concrete capacity. As a matter of fact, the concrete infill is well confined by the profiled stee sheet when internal fasteners are applied.

Table 2 Comparisons between test results and predicted results

Specimen No.	F_{test}	F_{AISC}	F_{Euro}	F_{CECS}	$F_{pro,k=0.8}$	$F_{pro,k=4.0}$	$F_{pro,k=5.467}$	$\frac{F_{test}}{F_{AISC}}$	$\frac{F_{test}}{F_{Euro}}$	$\frac{F_{test}}{F_{CECS}}$	$\frac{F_{test}}{F_{pro,k=0.8}}$	$\frac{F_{test}}{F_{pro,k=4.0}}$	$\frac{F_{test}}{F_{pro,k=5.467}}$
	kN	kN	kN	kN	kN	kN	kN						
DKCW-1	1330	949	1648	1847	1258	1345	1368	1.401	0.807	0.720	1.057	0.989	0.972
DKCW-2	1260	949	1648	1847	1258	1345	1368	1.328	0.765	0.682	1.00	0.937	0.921
DKCW-3	1480	1217	1907	2097	1517	1604	1627	1.216	0.776	0.706	0.976	0.923	0.910
Average								1.315	0.783	0.703	1.011	0.950	0.934
Standard deviation								0.076	0.018	0.016	0.034	0.028	0.027

Meanwhile, the comparison among the proposed methods using various values of elastic local buckling coefficient k shows that the predictions with $k = 0.8$ agree best with the test results. The mean value of the ratios of the test results to the predicted ones is 1.011, and the corresponding standard deviation is 0.034. This indicates that the boundary condition of the profiled steel sheets in composite wall is more likely to be simply-supported along loaded edges while free along the unloaded edges.

5. Conclusions

This paper presents the details of experiments conducted to investigate the structural performance of new profiled composite walls under compressive loading. The walls consist of two external profiled steel plates and concrete core inside. Two new types of fasteners are proposed to improve the structural behavior of the composite walls. The designed test specimens are subjected to axial compression. These tests offer information on the structural performance and failure modes of these specimens.

(1) Two failure modes are identified in the test. The first type of failure mode is featured with combined cracked concrete and vertical separation between steel plates and concrete core. This failure mode is observed in specimens with threaded rods. These specimens experienced local crushing of concrete, followed by the local buckling and crippling of profiled steel plates. The second type of failure mode is featured with the failure of cross-sectional capacity. The specimen with vertical plates provides good confinement to the profiled steel plates and both steel and concrete fully arrive at their carrying capacities.

(2) All specimens show similar axial load-axial deformation response. Good ductility and gradual reduction in load bearing capacity at increasing deformation can be achieved. Comparing to threaded rods, Vertical plates contribute more to the initial axial stiffness of the wall. Furthermore, specimens with thread rods do not fully utilize their cross-sectional capacity.

(3) Analysis on load-strain response indicates that vertical plate is the more suitable fastener type as it can prevent the profiled steel plate from premature buckling. Furthermore, threaded rods with symmetric arrangement is preferable to those with staggered arrangement as the former owns more stable axial strain developing during the whole loading process.

(4) The test results were compared with three modern codes and it was found that all codes did not well predict the actual capacity. A calculation method was then proposed and good agreement was achieved.

Acknowledgments

This work is sponsored by the Natural Science Foundation of Jiangsu Province (Grant No. BK20170685), the National Key Research and Development Program of China (Grant No. 2017YFC0703802), and the Fundamental Research Funds for the Central Universities. The authors would like to thank Jiangsu Xinlantian Steel Structure Co., Ltd. for the assistance with the test specimen fabrication.

References

AISC 360-16 (2016), Specification for structural steel buildings; American Institute of Steel Construction, Chicago, IL, USA.

Aykac, S., Kalkan, I. and Seydanlioglu, M. (2014), “Strengthening of hollow brick infill walls with perforated steel plates”, *Earthq. Struct., Int. J.*, **6**(2), 181-199.

Bqczkiewicz, J., Malaska, M., Pajunen, S. and Heinisuo, M. (2018), “Experimental and numerical study on temperature distribution of square hollow section joints”, *J. Constr. Steel Res.*, **142**, 31-43.

CECS 159 (2004), Technical specification for structures with concrete-filled rectangular steel tube members; China Association for Engineering Construction Standardization, Beijing, China.

Choi, J.Y. and Kwon, Y.B. (2018), “Direct strength method for high strength steel welded section columns”, *Steel Compos. Struct., Int. J.*, **29**(4), 509-526.

Choi, B.J., Kang, C.K. and Park, H.Y. (2014), “Strength and behavior of steel plate–concrete wall structures using ordinary and eco-oriented cement concrete under axial compression”, *Thin-Wall. Struct.*, **84**, 313-324.

Du, Y.S., Chen, Z.H. and Yu, Y.J. (2016), “Behavior of rectangular concrete-filled high-strength steel tubular columns with different aspect ratio”, *Thin-Wall. Struct.*, **109**, 304-318.

EN 1994-1-1 (2004), Eurocode 4: Design of composite steel and concrete structures-Part 1-1: General rules and rules for buildings; British Standards Institution, London, UK.

Epackachi, S., Whittaker, A.S. and Huang, Y.N. (2015), “Analytical modeling of rectangular SC wall panels”, *J. Constr. Steel Res.*, **105**, 49-59.

Garifullin, M., Launert, B., Heinisuo, M., Pasternak, H., Mela, K. and Pajunen, S. (2018), “Effect of welding residual stresses on local behavior of rectangular hollow section joints - Part 1- Development of numerical model”, *Bauingenieur*, **93**, 152-159.

GB50010-2010 (2015), Code for design of concrete structures; China Architecture & Building Press, Beijing, China.

Gerard, G. and Becker, M. (1957), *Handbook of Structural Stability: Part I-Buckling of Flat Plates*, National Advisory Committee for Aeronautics, New York University, USA.

Han, L.H. (2002), “Tests on stub columns of concrete-filled RHS sections”, *J. Constr. Steel Res.*, **58**(3), 353-372.

Hilo, S.J., Badaruzzaman, W.H.W, Osman, S.A. and Al-Zand, A.W. (2016), “Structural behavior of composite wall systems strengthened with embedded cold-formed steel tube”, *Thin Wall Struct.*, **98**, 607-616.

Hossain, K.M.A., Rafiei, S., Lachemi, M. and Behdinan, K. (2016), “Structural performance of profiled composite wall under in-plane cyclic loading”, *Eng. Struct.*, **110**, 88-104.

Huang, Z.Y. and Liew, J.Y.R. (2016), “Compressive resistance of steel-concrete-steel sandwich composite walls with J-hook connectors”, *J. Constr. Steel Res.*, **124**, 142-162.

Jamaluddin, N., Lam, D., Dai, X.H. and Ye, J. (2013), “An experimental study on elliptical concrete filled columns under axial compression”, *J. Constr. Steel Res.*, **87**, 6-16.

Liang, Q.Q. and Uy, B. (2000), "Theoretical study on the post-local buckling of steel plates in concrete-filled box columns", *Comput. Struct.*, **75**, 479-490.
Liang, Q.Q., Uy, B., Wright, H.D. and Bradford, M.A. (2004), "Local buckling of steel plates in double skin composite panels under biaxial compression and shear", *J. Struct. Eng.*, **130**(3), 443-451.
Liu, Z.A., Liu, H.B., Chen, Z.H. and Zhang, G.P. (2018), "Structural behavior of cold-formed thick-walled rectangular steel columns", *J. Constr. Steel Res.*, **147**, 277-292.
Mydin, M.A.O. and Wang, Y.C. (2011), "Structural performance of lightweight steel-foamed concrete-steel composite walling system under compression", *Thin-Wall. Struct.*, **49**, 66-76.
Prabha, P., Marimuthu, V., Saravanan, M., Palani, G.S., Lakshmanan, N. and Senthil, R. (2013), "Effect of confinement on steel-concrete composite light-weight load-bearing wall panels under compression", *J. Constr. Steel Res.*, **81**, 11-19.
Qin, Y. and Chen, Z.H. (2016), "Research on cold-formed steel connections: A state-of-the-art review", *Steel Compos. Struct., Int. J.*, **20**(1), 21-41.
Qin, Y., Chen, Z.H. and Rong, B. (2015a), "Component-based mechanical models for concrete-filled RHS connections with diaphragms under bending moment", *Adv. Struct. Eng.*, **18**(8), 1241-1255.
Qin, Y., Chen, Z.H. and Rong, B. (2015b), "Modeling of CFRT through-diaphragm connections with H-beams subjected to axial load", *J. Contr. Steel Res.*, **114**, 146-156.
Qin, Y., Chen, Z.H., Bai, J.J. and Li, Z.L. (2016), "Test of extended thick-walled through-diaphragm connection to thick-walled CFT column", *Steel Compos. Struct., Int. J.*, **20**(1), 1-20.
Qin, Y., Shu, G.P., Fan, S.G., Lu, J.Y., Cao, S. and Han, J.H. (2017a), "Strength of double skin steel-concrete composite walls", *Int. J. Steel Struct.*, **17**(2), 535-541.
Qin, Y., Lu, J.Y. and Cao, S. (2017b), "Theoretical study on local buckling of steel plate in concrete filled tube column under axial compression", *ISIJ Int.*, **57**(9), 1645-1651.
Qin, Y., Zhang, J.C., Shi, P., Chen, Y.F., Xu, Y.H. and Shi, Z.Z. (2018a), "Behavior of improved through-diaphragm connection to square tubular column under tensile loading", *Struct. Eng. Mech., Int. J.*, **68**(4), 475-483.
Qin, Y., Shu, G.P., Du, E.F. and Lu, R.H. (2018b), "Buckling analysis of elastically-restrained steel plates under eccentric compression", *Steel Compos. Struct., Int. J.*, **29**(3), 379-389.
Qin, Y., Du. E.F., Li, Y.W. and Zhang, J.C. (2018c), "Local buckling of steel plates in composite structures under combined bending and compression", *ISIJ Int.*, **58**(11), 2133-2141.
Qin, Y., Shu, G.P., Zhou, X.L., Han, J.H. and He, Y.F. (2019a), "Height-thickness ratio on axial behavior of composite wall with truss connector", *Steel Compos. Struct., Int. J.*, **30**(4), 315-325.
Qin, Y., Shu, G.P., Zhou, G.G. and Han, J.H. (2019b), "Compressive behavior of double skin composite wall with different plate thickness", *J. Constr. Steel Res.*, **157**, 297-313.
Qin, Y., Li, Y.W., Su, Y.S., Lan, X.Z., Wu, Y.D. and Wang, X.Y. (2019c), "Compressive behavior of profiled double skin composite walls", *Steel Compos. Struct., Int. J.*, **30**(5), 405-416.
Rafiei, S., Hossain, K.M.A., Lachemi, M., Behdinan, K. and Anwar, M.S. (2013), "Finite element modeling of double skin profiled composite shear wall system under in-plane loadings", *Eng. Struct.*, **56**, 46-57.
Ritchie, C.B., Packer, J.A., Seica, M.V., Zhao, X.L. (2018), "Behaviour and analysis of concrete-filled rectangular hollow sections subject to blast loading", *J. Constr. Steel Res.*, **147**, 340-359.
Sakr, M.A., El-Khoriby, S.R., Khalifa, T.M. and Nagib, M.T. (2017), "Modeling of RC shear walls strengthened by FRP composites", *Struct. Eng. Mech., Int. J.*, **61**(3), 407-417.
Shekastehband, B., Mohammadbagheri, S. and Taromi, A. (2018), "Seismic behavior of stiffened concrete-filled double-skin tubular columns", *Steel Compos. Struct., Int. J.*, **27**(5), 577-598.
Shen, J.J. and Wadee, M.A. (2018), "Imperfection sensitivity of thin-walled rectangular hollow section struts susceptible to interactive buckling", *Int. J. Nonlin. Mech.*, **99**, 112-130.
Tao, Z., Han, L.H. and Zhao, X.L. (1998), "Bahaviour of square concrete filled tubes subjected to axial compression", *Proceedings of the Fifth International Conference on Structural Engineering for Young Experts*, Shenyang, China.
Uy, B. and Bradford, M.A. (1996), "Elastic local buckling of steel plates in composite steel-concrete members", *Eng. Struct.*, **18**, 193-200.
Uy, B., Wright, H.D. and Bradford, M.A. (2001), "Combined axial and flexural strength of profiled composite walls", *Proc. Inst. Civil Eng.-Struct. Build.*, **146**(2), 129-139.
Wright, H. (1998), "The axial load behavior of composite walling", *J. Constr. Steel Res.*, **45**(3), 353-375.
Xiong, Q.Q., Chen, Z.H., Zhang, W., Du, Y.S., Zhou, T. and Kang, J.F. (2017), "Compressive behaviour and design of L-shaped columns fabricated using concrete-filled steel tubes", *Eng. Struct.*, **152**, 758-770.
Yan, J.B., Wang, Z., Wang, T. and Wang, X.T. (2018), "Shear and tensile behaviors of headed stud connectors in double skin composite shear wall", *Steel Compos. Struct., Int. J.*, **26**(6), 759-769.
Yousefi, M. and Ghalehnovi, M. (2018), "Finite element model for interlayer behavior of double skin steel-concrete-steel sandwich structure with corrugated-strip shear connectors", *Steel Compos. Struct., Int. J.*, **27**(1), 123-133.
Zhang, K., Varma, A.H., Malushte, S.R. and Gallocher S. (2014), "Effect of shear connectors on local buckling and composite action in steel concrete composite walls", *Nucl. Eng. Des.*, **269**, 231-239.
Zhang, T., Ding, F.X., Wang, L.P., Liu, X.M. and Jiang, G.S. (2018), "Behavior of polygonal concrete-filled steel tubular stub columns under axial loading", *Steel Compos. Struct., Int. J.*, **28**(5), 573-588.

CC